Energy & Environmental Science

ROYAL SOCIETY OF CHEMISTRY

PAPER

View Article Online
View Journal | View Issue

Cite this: *Energy Environ. Sci.*, 2023, **16**, 2080

Reduced 0.418 V V_{OC}-deficit of 1.73 eV wide-bandgap perovskite solar cells assisted by dual chlorides for efficient all-perovskite tandems†

Yue Zhao,‡[ab] Changlei Wang,‡*[ab] Tianshu Ma,[ab] Luwei Zhou,[ab] Zhanghao Wu,[ab] Huayang Wang,[ab] Cong Chen,[c] Zhenhua Yu,[d] Weiwei Sun,[e] Aolin Wang,[f] Hao Huang,[f] Bingsuo Zou,[f] Dewei Zhao*[c] and Xiaofeng Li*[ab]

Received 19th December 2022,
Accepted 14th March 2023

DOI: 10.1039/d2ee04087e

rsc.li/ees

Wide-bandgap (wide-E_g) perovskites with bandgaps over 1.65 eV have great potential for constructing tandem solar cells (TSCs); however, they still suffer from large open-circuit voltage (V_{OC}) deficits. Phase segregation and non-radiative recombination are great challenges for inverted wide-E_g perovskite solar cells (PSCs) to achieve an ideal V_{OC} and long-term operation stability. Herein, we report a synergistic strategy of using lead chloride ($PbCl_2$) and phenethylammonium chloride (PMACl) to introduce chlorine (Cl) into a bulk film and form a two-dimensional (2D) phase at the film surface for 1.73 eV wide-E_g PSCs, which reduce the V_{OC}-deficit from 0.558 V to 0.418 V. Cl in $PbCl_2$ enters the crystal lattice of the perovskite film, reducing the halide vacancies and suppressing ion migration. Meanwhile, PMACl facilitates the formation of a 2D perovskite phase at the grain surfaces, alleviating recombination and improving the stability. As a result, the best-performing wide-E_g PSC with a high V_{OC} of 1.312 V and an efficiency of over 20% is achieved, enabling the fabrication of two-terminal all-perovskite TSCs with a champion efficiency of 26.68%. This work provides in-depth insights into how Cl suppresses phase segregation and non-radiative recombination in wide-E_g PSCs, offering a promising strategy for efficient and stable all-perovskite TSCs.

Broader context

Perovskite solar cells (PSCs) are considered one of the most promising candidates for next-generation photovoltaic technology applications due to their high power conversion efficiencies (PCEs) and low-cost fabrication processes. Currently, the PCE of a single-junction PSC has been boosted to 25.7%, approaching the Shockley–Queisser efficiency limit. Constructing an all-perovskite tandem solar cell (TSC) is an effective route to further enhance the photovoltaic performance of PSCs. However, wide-E_g (>1.65 eV) PSCs still suffer from unsatisfactory performance with large V_{OC}-deficits (defined as $E_g/q - V_{OC}$, where q is the elementary charge) and inferior stability, which can be related to the phase segregation and non-radiative recombination. Herein, we report a facile dual chloride additive route to fabricate high-quality wide-E_g perovskite absorbers with alleviated non-radiative recombination, suppressed phase segregation, and improved stability through the synergistic effects of lead chloride ($PbCl_2$) and phenethylammonium chloride (PMACl). We also uncover the mechanisms underlying how chlorides suppress the phase segregation and non-radiative recombination in wide-E_g PSCs. At last, high-performance single-junction 1.73 eV wide-E_g PSCs with over 20% efficiencies and V_{OC}-deficits as low as 0.418 V are achieved, enabling the fabrication of all-perovskite TSCs with a champion PCE of 26.68%.

[a] *School of Optoelectronic Science and Engineering & Collaborative Innovation Center of Suzhou Nano Science and Technology, Soochow University, Suzhou 215006, China. E-mail: cl.wang@suda.edu.cn, xfli@suda.edu.cn*

[b] *Key Lab of Advanced Optical Manufacturing Technologies of Jiangsu Province & Key Lab of Modern Optical Technologies of Education Ministry of China, Soochow University, Suzhou 215006, China*

[c] *College of Materials Science and Engineering, Engineering Research Center of Alternative Energy Materials & Devices, Ministry of Education, Sichuan University, Chengdu 610065, China. E-mail: dewei_zhao@hotmail.com, dewei.zhao@scu.edu.cn*

[d] *Key Laboratory of Artificial Micro- and Nano-structures of Ministry of Education of China, School of Physics and Technology, Wuhan University, Wuhan 430072, China*

[e] *College of Aerospace Science and Engineering, National University of Defense Technology, Changsha 410073, China*

[f] *Guangxi Key Laboratory of Processing for Non-ferrous Metals and Featured Materials, School of Resources, Environments and Materials, Guangxi University, Nanning 530004, China*

† Electronic supplementary information (ESI) available. See DOI: https://doi.org/10.1039/d2ee04087e

‡ These authors contributed equally.

1. Introduction

Organic metal halide perovskites are promising materials for next-generation photovoltaics owing to their unique optoelectronic properties, such as high absorption coefficients, long carrier diffusion lengths, and low-cost solution processability.[1,2] Single-junction perovskite solar cells (PSCs) have gained tremendous development in the past decade with the power conversion efficiency (PCE) boosted to the certified value 25.7%.[3] Further improving the performance of single-junction PSCs is challenging and limited by the Shockley–Queisser (S–Q) radiative efficiency.[4]

Tandem solar cells (TSCs) hold a higher theoretical efficiency than single-junction cells by reducing thermalization losses.[5,6] Perovskites have a wide bandgap tunability from 1.2 to 3.0 eV, which makes them suitable for all-perovskite TSCs.[7–10] A typical double-junction TSC usually consists of a wide-E_g top subcell and a low-E_g bottom subcell, which should have matched current densities between the two subcells for a monolithic configuration.[11] Currently, the short-circuit current density (J_{SC}) of high-efficiency all-perovskite TSCs has largely increased by the growth of over 1 micrometer thick low-E_g absorber layers.[12] However, the open-circuit voltage (V_{OC}) of TSCs is still lower than their theoretical limit, which might be ascribed to large voltage losses of the subcells, especially for the top subcell with a large amount of bromine (Br) leading to phase segregation.[13,14] The mixture of iodine (I) and Br usually suffers from severe phase segregation and inferior energy level alignment in wide-E_g PSCs, leading to unsatisfactory V_{OC} losses.[14–17] Introducing lead chloride ($PbCl_2$) into wide-E_g perovskites to form triple-halide compositions could alleviate the phase segregation, thus significantly improving the V_{OC} and performance of wide-E_g PSCs and their corresponding perovskite/Si tandem cells.[18] Therefore, it is highly desired to uncover the roles of chlorine (Cl) in wide-E_g perovskites and reduce the V_{OC}-deficits (defined as $E_g/q - V_{OC}$, where q is the elementary charge) to further improve the performance of single-junction PSCs and all-perovskite TSCs.

Strategies such as interface passivation and dimensional tailoring have also been proposed to reduce the V_{OC}-deficits in wide-E_g PSCs.[17,19–22] Adding a small amount of large organic cations to three-dimensional (3D) perovskites can help form the two-dimensional (2D) and quasi-2D phases at the grain surface, which could simultaneously eliminate the defects and improve the stability of PSCs.[23,24] Organic spacers, such as phenylethylamine (PEA^+) and butylammonium (BA^+), have been proved to be efficient passivators in perovskite films.[25] Several Cl-containing additives, such as ammonium chloride (NH_4Cl) and methylammonium chloride (MACl), have also been employed in precursors to enhance the perovskite crystallinity.[26,27] However, the passivation effects of chlorides on wide-E_g perovskite films have rarely been investigated, especially in all-perovskite TSCs suffering from large V_{OC}-deficits.

In this work, we report a synergistic strategy of simultaneously incorporating $PbCl_2$ and phenylalkylamine chloride (PMACl) additives into a 1.73 eV wide-E_g perovskite precursor to effectively improve the film quality. Cl in $PbCl_2$ entering the perovskite lattice forms a triple-halide perovskite film with suppressed phase segregation. Meanwhile, PMA^+ could effectively reduce the surface defects and improve the film stability with 2D perovskite phases without sacrificing the carrier extraction dynamics. As a result, the highest V_{OC} of 1.312 V is achieved in our 1.73 eV PSCs, delivering a V_{OC}-deficit as low as 0.418 V, which is among the lowest values of wide-E_g PSCs reported so far. These enable the fabrication of two-terminal (2T) all-perovskite TSCs with a champion PCE of 26.68% by integrating an efficient wide-E_g subcell with a low-E_g tin–lead (Sn–Pb) bottom subcell, as well as improved operational stability of remaining 85% of the initial efficiency after continuous illumination for 300 h.

2. Results and discussion

2.1 Photovoltaic performance of single-junction wide-E_g PSCs

We introduced chloride additives into the wide-E_g perovskite precursors through compositional engineering with certain amounts of $PbCl_2$, PMACl, and a mixture of $PbCl_2$ and PMACl (referred to as $PbCl_2$ + PMACl). The introduction of chloride additives has little effect on the bandgaps of perovskite films, as shown in Fig. S1 (ESI†), possibly due to the formation of trace amounts of triple halides (I, Br, and Cl) in the final absorber layers.[18] Because the bandgap variation is less than 0.005 eV in perovskite films with and without Cl addition, we unified the bandgaps of all perovskites as 1.73 eV.

We first investigated the effects of additive concentration on the film quality and device performance. Single-junction wide-E_g PSCs were prepared with an inverted structure of ITO/PTAA/PFNBr/perovskite/C_{60}/BCP/Cu, where PTAA is poly[bis(4-phenyl)(2,4,6-trimethylphenyl)amine], PFNBr is poly[(9,9-bis(3′-(*N*,*N*-dimethyl)-*N*-ethylammonium-propyl)-2,7-fluorene)-*alt*-2,7-(9,9-dioctylfluorene)]dibromide, and BCP is bathocuproine. The optimal concentration of $PbCl_2$ and PMACl was 1 mol% for both types of PSCs (Fig. S2–S7 and Tables S1, S2, ESI†).[28] We further optimized the $PbCl_2$ + PMACl (with a ratio of 1 : 1) content in PSCs and obtained the optimal concentration of 1 mol% (Fig. S8–S10 and Table S3, ESI†), because the overdose led to relatively smaller grains with pin-holes and lower photoluminescence (PL) responses (Fig. S11, ESI†).[29]

The representative current density–voltage (J–V) curves of single-junction PSCs with different additives are shown in Fig. 1a and Table S4 (ESI†). The control PSC has a V_{OC} of 1.172 V, a J_{SC} of 18.14 mA cm^{-2}, and a fill factor (FF) of 81.7%, yielding a PCE of 17.38%. After $PbCl_2$ incorporation, the device has a highly increased FF to 83.2%, leading to a PCE of 18.19% with a V_{OC} of 1.201 V and a J_{SC} of 18.19 mA cm^{-2}. The PMACl device also shows a significant improvement in both V_{OC} and J_{SC} to 1.278 V and 18.55 mA cm^{-2}, respectively, thus leading to a PCE of 19.22%. The $PbCl_2$ + PMACl device merges the advantages of two additives and achieves the highest PCE of 20.22%, along with a V_{OC} of 1.312 V, a J_{SC} of 18.89 mA cm^{-2}, and a FF of 81.6%.

The statistics of photovoltaic parameters of wide-E_g PSCs with different additives are shown in Fig. 1b and c and summarized in Table S5 (ESI†). It is clear that the V_{OC}s are significantly enhanced after chloride addition. The $PbCl_2$ +

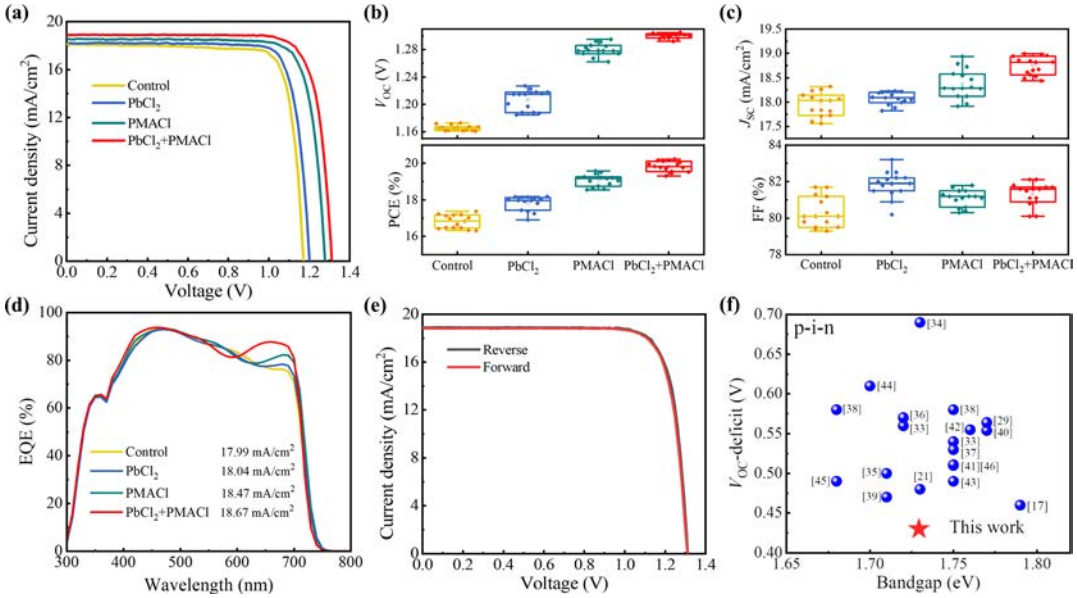

Fig. 1 Photovoltaic performance of wide-E_g PSCs with different additives. (a) J–V curves of wide-E_g PSCs with different additives. Statistical results of (b) V_{OC} and PCE, (c) J_{SC} and FF of wide-E_g PSCs. The results are calculated from 20 individual devices. (d) EQE plots of wide-E_g PSCs with various additives. (e) J–V curves of the champion wide-E_g PSC under reverse and forward scans. (f) V_{OC}-deficit values of inverted wide-E_g PSCs with bandgaps ranging from 1.68 to 1.79 eV reported in the literature.

PMACl co-modified PSCs exhibit the highest average V_{OC} of 1.301 ± 0.011 V compared to the others, indicating the best film quality with less energy loss. The FF is slightly improved to over 80% for Cl-modified devices. The J_{SC} gradually increases with the order of control, $PbCl_2$, PMACl, and $PbCl_2$ + PMACl, demonstrating improved light absorption. As a result, the synergistic effects of $PbCl_2$ and PMACl boost the overall PCEs of wide-E_g PSCs to 19.83 ± 0.53% (Table S5, ESI†).

The corresponding external quantum efficiency (EQE) plots and integrated J_{SC} values of four devices are shown in Fig. 1d. The integrated J_{SC}s are consistent with the J_{SC} values obtained from the J–V curves. It is interesting to notice that the EQE response at the wavelength region from 600 to 700 nm gradually increases after Cl introduction, contributing to the increasing trend of J_{SC}. We attribute this to the better passivation effect of Cl incorporation in perovskite films with fewer defects, especially at the rear interfaces with reduced non-radiative recombination and improved charge collection.[30,31]

Fig. 1e shows an optimized single-junction wide-E_g PSC presenting negligible hysteresis, and the J–V details of other PSCs are shown in Fig. S12 and Table S4 (ESI†). A power output of 20.1% was recorded using maximum power point (MPP) tracking under AM 1.5G illumination (Fig. S13, ESI†). The V_{OC} of the optimized device reaches 1.312 V, leading to a V_{OC}-deficit of 0.418 V, which is among the lowest values for inverted wide-E_g PSCs with bandgaps ranging from 1.68 to 1.79 eV for potential application in all-perovskite TSCs to date (Fig. 1f and Table S6, ESI†).[15,17,21,29,32–46]

2.2 Morphology and optoelectronic properties of wide-E_g perovskite films

The morphology and optoelectronic properties of wide-E_g perovskite films are scrutinized to unveil the underlying mechanisms for device performance enhancement. Fig. 2a shows the scanning electron microscopy (SEM) images of four samples. The averaged crystal size is almost the same for the control (173 nm) and PMACl (176 nm) samples, while it becomes slightly larger to 196 and 191 nm for $PbCl_2$ and $PbCl_2$ + PMACl films, respectively (Fig. S14 and S15, ESI†). As shown in Fig. S16 (ESI†), the root mean square (RMS) roughness values are 32.8, 35.9, 18.5, and 26.0 nm for the control, $PbCl_2$, PMACl, and $PbCl_2$ + PMACl films, respectively. The $PbCl_2$ film has the largest roughness possibly due to the formation of PbI_2 particles at the film surface. The PMACl and $PbCl_2$ + PMACl films have relatively smoother surfaces, which should be ascribed to the surface polishing effect of PMACl triggering the formation of a 2D phase at the film surface.[28,31]

In order to dig out the fundamental mechanisms of the crystallization and passivation processes, we measured the X-ray diffraction (XRD) patterns of the films with different additives and concentrations (Fig. 2b and Fig. S17–S19, ESI†). $PbCl_2$ treatment induces the most pronounced peak around 12.8° representing PbI_2, consistent with the SEM images with bright particles. We further confirmed the compositions of these bright particles as generated PbI_2 *via* energy dispersive spectroscopy (EDS) measurements (Fig. S17, ESI†). Moreover, the (110) main diffraction peak at around 20° slightly shifts to a larger angle upon more Cl treatments, indicating the shrinkage of the crystal lattice (Fig. S18, ESI†), which should be ascribed to the successful incorporation of Cl into the perovskite framework.[47]

We speculate that the PMA^+ organic cations with a large molecular size are likely inserted into the layered PbX_2 (X = I, Br, and Cl) framework, forming 2D phases of $(PMA)_2A_{n-1}Pb_nX_{3n+1}$ at the grain surfaces, where A is FA and Cs; X is I, Br, and Cl; and n is the layer number.[48–50] A corresponding schematic of the

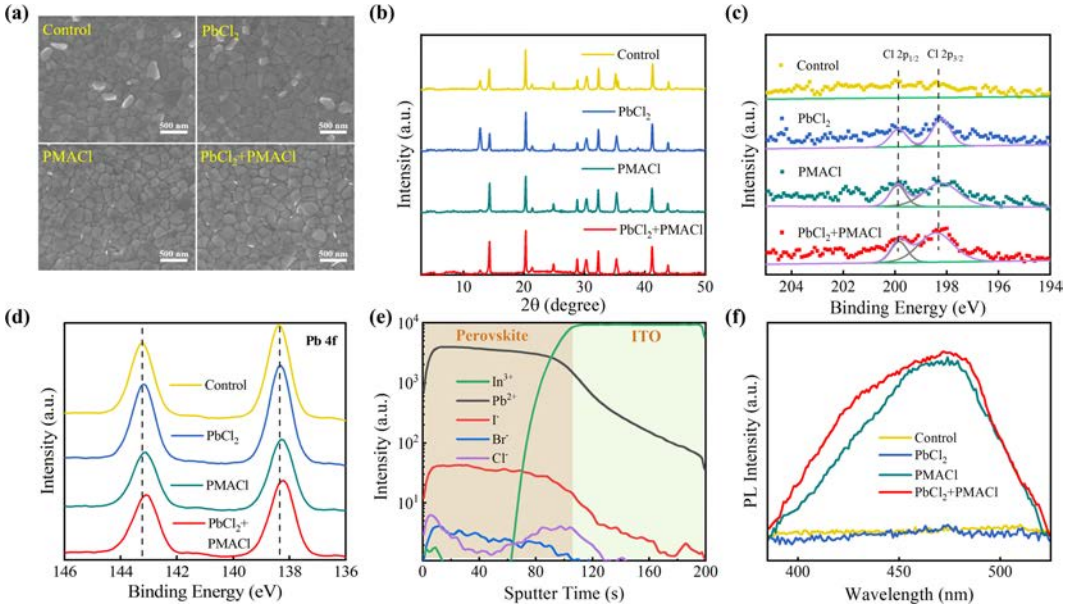

Fig. 2 Film quality and compositional properties of wide-E_g perovskites. (a) Top-view SEM images of wide-E_g perovskite films with different additives. (b) XRD patterns of perovskite films with various additives. XPS spectra of (c) Cl 2p and (d) Pb 4f orbitals in different perovskite films. (e) ToF-SIMS profiles of the $PbCl_2$ + PMACl perovskite film. (f) PL spectra of wide-E_g perovskite films with different additives.

mechanisms of the 2D phase formation is displayed in Fig. S19 (ESI†). At a low concentration of PMACl, the amount of 2D phase is likely too low to be detected using XRD characterization (Fig. S20, ESI†). By increasing the concentration of different additives, obvious quasi-2D (n = 2, $(PMA)_2APb_2X_7$) and/or 2D (n = 1, $(PMA)_2PbX_4$) phases were obtained in the PMACl-presented films, as shown in Fig. S21 (ESI†). The $PbCl_2$-incorporated films show no 2D peaks, while the PMACl samples show clear quasi-2D (*i.e.*, $(PMA)_2APb_2X_7$) peaks at higher additive concentrations (>5 mol%), consistent with those in previous reports.[51,52] More interestingly, the $PbCl_2$ + PMACl films begin to show the 2D phase ($(PMA)_2PbX_4$) at a certain concentration of 5 mol%; however, the 2D phase changes to a quasi-2D phase ($(PMA)_2APb_2X_7$) with an increase in the $PbCl_2$ + PMACl concentration. Combined with the aforementioned film surface morphology and device performance, we suppose that a thin layer of 2D phase could passivate the defects and improve the device performance, while a thick 2D layer would sacrifice the device efficiency due to insufficient charge transfer dynamics.

We performed X-ray photoelectron spectroscopy (XPS) to check the compositions of the perovskite films. As shown in Fig. 2c, the control film has no signal of Cl, while the others present distinguishable Cl elements, indicating the incorporation of Cl into the target films.[53] Fig. 2d shows that the Pb 4f peak shifts to the lower energy region after treatments, indicating the reduced defects of uncoordinated Pb ions.[12,54] It is easy to form iodine vacancies in the perovskite lattice, while the presence of Br could alleviate the halide defects due to the combination with uncoordinated Pb.[55] The introduction of Cl could further reduce the halide vacancies because of the higher electronic negativity.[56] Therefore, the combination of triple halides and 2D-phase surfaces simultaneously passivates the traps and inhibits ion migration, leading to improved crystallinity and quality of wide-E_g perovskite films.

Furthermore, in order to detect the location of Cl in the final films, we investigated the cross-sectional distribution profiles of the control and optimal $PbCl_2$ + PMACl films through time-of-flight secondary ion mass spectrometry (ToF-SIMS) measurements (Fig. S22, ESI† and Fig. 2e). The control sample has no Cl in the bulk, while for the $PbCl_2$ + PMACl film, Cl distributes in the whole region across the film in the presence of both I and Br, confirming the coexistence of triple halides in the film.[18] Moreover, Cl is more prominent at the bottom and top perovskite/charge transporting layer (CTL) interfaces, indicating that Cl is accumulated at two surfaces due to the presence of a large number of defects that are favorable to bond with the additives.[27] The presence of Cl at the interface of perovskite/CTLs could further release the lattice strains, thus reducing the defects and suppressing the phase segregation.[47]

To further confirm the 2D perovskite phases at the film surface, PL spectra were recorded at the short wavelength region around 480 nm (Fig. 2f).[22] The control and $PbCl_2$ films show no emission peaks, implying the absence of 2D phases. However, the PMACl and $PbCl_2$ + PMACl films show a characteristic peak, indicating the existence of 2D and quasi-2D perovskites at the grain surfaces or grain boundaries, consistent with the XRD results discussed above.[27]

PL and transient PL (TRPL) measurements were conducted to investigate the charge dynamics in wide-E_g perovskites upon Cl treatment. As shown in Fig. 3a and b, the $PbCl_2$ + PMACl film has the strongest PL intensity and the longest carrier lifetime of 209 ns compared to others, indicating the most suppressed nonradiative recombination and reduced trap density upon the synergistic effects of PMACl and $PbCl_2$. In addition, the carrier

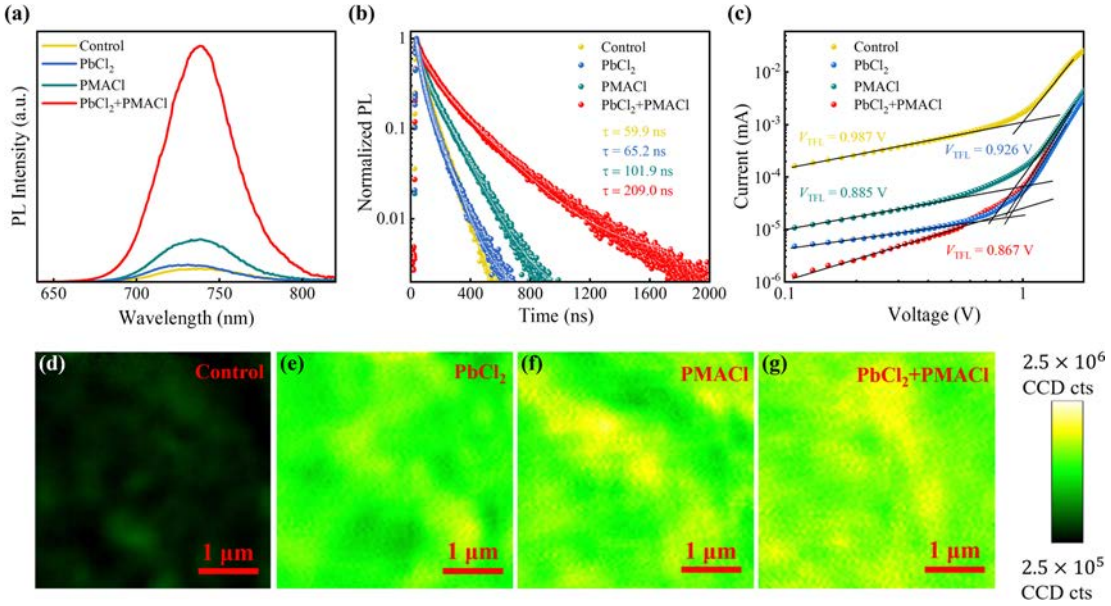

Fig. 3 Optoelectronic properties of wide-E_g perovskites. (a) PL and (b) TRPL spectra of wide-E_g perovskite films with different additives. (c) J–V curves of electron-only devices with different additives based on the SCLC protocol. (d–g) PL mapping images of wide-E_g perovskite films upon different treatments.

lifetimes of $PbCl_2$ and PMACl films are slightly prolonged to 65.2 and 101.9 ns, respectively, compared to the control one of 59.9 ns (Fig. 3b and Table S7, ESI†), suggesting the insufficient passivation by solely chloride addition.

Since wide-E_g perovskites are vulnerable to phase segregation, we further monitored the phase stability of films with different additives upon aging. The PL spectra of four samples after 10 days of storage are shown in Fig. S23 (ESI†). The control sample shows obvious phase separation with two emission peaks, which should be ascribed to the segregated I-rich and Br-rich phases.[57] Although $PbCl_2$ or PMACl individually added film has a relatively higher PL intensity than the control one (Fig. S23a, ESI†), they still suffer from halide separation with two distinguishable emission peaks at 717 and 758 nm (Fig. S23b, ESI†), possibly triggered by halide vacancies and ion migration.[18,57] Meanwhile, the $PbCl_2$ + PMACl film shows negligible phase segregation with just one peak. We attribute the suppressed phase segregation to the effective passivation of dual chlorides, making them less vulnerable to ion migration.[43,55]

Moreover, we used the space charge limited current (SCLC) characterization to evaluate the trap density in perovskite films based on the electron-only devices with the structure ITO/SnO_2/perovskite/PCBM/Cu. The trap-filled limit voltage (V_{TFL}) value of 0.867 V for the $PbCl_2$ + PMACl device is the smallest compared to the others, implying the lowest trap density in the optimized wide-E_g films upon dual chloride addition.[58] The SCLC measurements of the hole-only devices also confirmed the lowest defect level in the $PbCl_2$ + PMACl film (Fig. S24, ESI†), since they show a similar trend of V_{TFL} values to that of electron-only devices. Fig. S25 (ESI†) shows the J–V curves of PSCs with different additives under dark conditions. The $PbCl_2$ + PMACl device has the lowest dark current, indicating reduced current leakage.[59,60]

We further conducted the PL mapping to investigate the surface homogeneity of perovskite films, as shown in Fig. 3d–g. Perovskite films with homogeneous surfaces have retarded phase transitions due to suppressed elementary aggregation.[61] The control film without any additive shows the lowest response with nonuniformity, indicating the severe nonradiative recombination of charge carriers and inferior film homogeneity.[29] Both $PbCl_2$ and PMACl films show relatively brighter emission color, indicating improved film quality with reduced defects.[53] However, they still have dark regions at the film surface, indicating compositional inhomogeneity, which is detrimental to the phase stability. On the other hand, the $PbCl_2$ + PMACl film shows the brightest color and a more homogeneous surface, implying the best film quality with uniform elementary distribution, fewer defects, and suppressed nonradiative recombination.[62]

2.3 Charge transfer dynamics and stability of wide-E_g perovskite films and devices

Fig. 4a shows the Mott–Schottky plots extracted from the capacitance–voltage (C–V) measurements for wide-E_g PSCs.[63] The $PbCl_2$ + PMACl device has a relatively higher built-in voltage of 0.875 V than the control (0.674 V), $PbCl_2$ (0.683 V), and PMACl (0.859 V) devices, indicating the highest built-in potential that favors charge separation and transportation. This is consistent with the V_{OC} trend. These results indicate that the synergistic effects of two additives reduce the defects and improve the charge transfer dynamics.[62]

We also characterized the light intensity dependence of V_{OC} and J_{SC} to investigate the charge recombination and transfer in wide-E_g PSCs. The V_{OC} plots of PSCs as a function of light intensity are depicted in Fig. 4b. The V_{OC} follows a linear relationship with the logarithmic light intensity according to $V_{OC} = (nk_BT/q)\ln(I/I_0 + 1)$, where k_B is the Boltzmann constant,

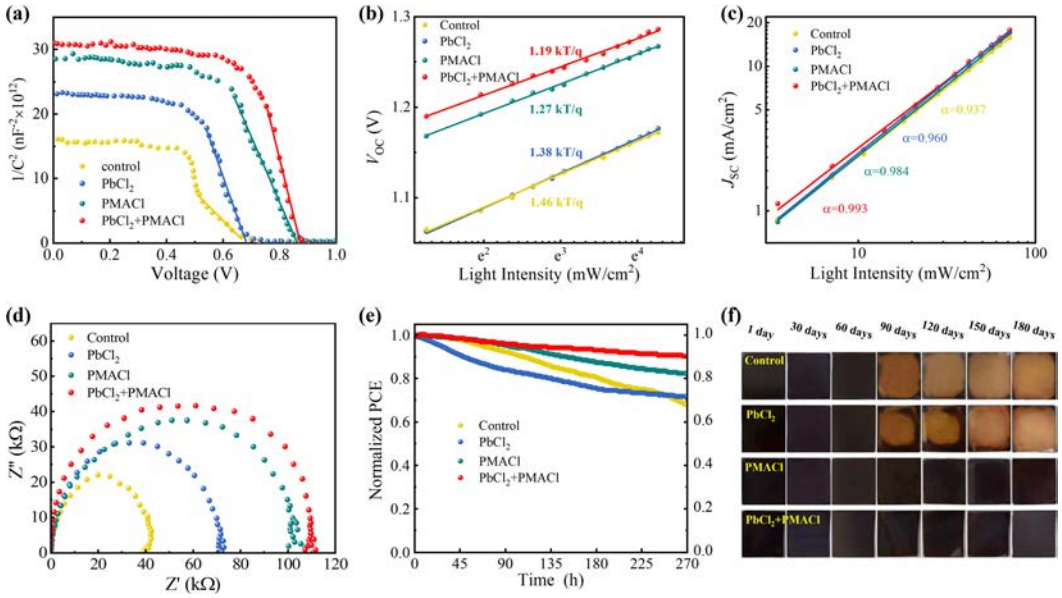

Fig. 4 Charge transfer dynamics and stability of wide-E_g PSCs. (a) Mott–Schottky plots from C–V measurements for wide-E_g PSCs with different treatments. (b) V_{OC} and (c) J_{SC} of wide-E_g PSCs as a function of light intensity. (d) Nyquist plots of wide-E_g PSCs with different additives. (e) Normalized PCEs *versus* time under MPP tracking at 1 sun illumination for wide-E_g PSCs with different additives. The devices without encapsulation were measured under 100 mW cm^{-2} with a LED light source and under inert conditions. (f) Color evolution images of wide-E_g perovskite films with different treatments aged for 180 days under ambient conditions.

T is the temperature, and n is the ideal factor. The n values are calculated to be 1.46, 1.38, 1.27, and 1.19 for the control, $PbCl_2$, PMACl, and $PbCl_2$ + PMACl devices, respectively. The smallest n value for the $PbCl_2$ + PMACl device suggests the lowest Shockley–Read–Hall (SRH) recombination,[64] in good agreement with the reduced trap density and prolonged carrier lifetime as mentioned above. The J_{SC} plots as a function of light intensity are depicted in Fig. 4c. The J_{SC} follows a linear relationship with I^{α}, where I is the light intensity. The control PSC has an α of 0.937, while the $PbCl_2$ device and the PMACl device have higher values of 0.969 and 0.984, respectively. The $PbCl_2$ + PMACl device has the highest value of 0.993 close to 1, indicating the largely reduced space charge limited current.[65]

Electrochemical impedance (EIS) spectra were further scrutinized to investigate the charge transfer dynamics in PSCs (Fig. 4d), and an equivalent fitting circuit is shown in Fig. S26 (ESI†). A larger semicircle of the Nyquist plot indicates a bigger recombination resistance.[30] The $PbCl_2$ + PMACl target device has the largest semicircle compared to the others, indicating fluent charge transfer with less nonradiative recombination.[63]

Fig. 4e shows the power outputs of wide-E_g PSCs measured using MPP tracking in a glovebox under 1 sun illumination. The control device shows a sharp performance degradation with only 65% of its initial efficiency retained after 270 h. The $PbCl_2$ device and the PMACl device retained 71% and 81% of their original values, respectively. The $PbCl_2$ + PMACl target device showed an enhanced operational stability of retaining 90% of its initial efficiency after 270 h of illumination. Such operational stability is comparable with those reported ones of wide-E_g PSCs with mixed halides.[61] The improved stability should be ascribed to the suppressed defects and phase segregation of the perovskite film with dual Cl additives incorporated.[66]

We further monitored the long-term stability of wide-E_g perovskite films upon ambient exposure for 180 days with a relative humidity of around 60% and a temperature of about 20 °C (Fig. 4f). The control device and the $PbCl_2$ device showed fast degradation that decomposed to white color within 90 days, indicating the inferior stability vulnerable to moisture and oxygen. However, the PMACl device and the $PbCl_2$ + PMACl device retain dark color with negligible change after 180 days of exposure, possibly due to the presence of a thin layer of 2D perovskites, which could effectively impede the permeation of moisture and oxygen and thus inhibit the decomposition of perovskites.[67] This is also evidenced by the well-maintained compact film surface and sharp absorption onset around 730 nm of the PMACl and $PbCl_2$ + PMACl films (Fig. S27 and S28, ESI†), indicating the well-remaining perovskite phase. These results further confirm the important role of 2D perovskite passivation in improving the film quality with reduced trap density and increased stability.[66] We also checked the long-term stability of wide-E_g PSCs in the N_2-filled glovebox (Fig. S29, ESI†). The $PbCl_2$ + PMACl device retains 89% of its original efficiency after 135 days of shelf storage under an N_2 atmosphere.

2.4 Photovoltaic performance of 2T all-perovskite TSCs

We prepared 2T all-perovskite TSCs with the architecture ITO/PTAA/PFNBr/wide-E_g perovskite/C_{60}/SnO_2/ITO/PEDOT:PSS/low-E_g perovskite/C_{60}/BCP/Cu, relying on the optimized wide-E_g perovskite subcells paired with the 1.25 eV low-E_g Sn–Pb bottom subcells, where PEDOT:PSS is poly(3,4-ethylenedioxythiophene):polystyrene sulfonate. The photovoltaic performance of single-junction low-E_g

PSCs is shown in Fig. S30 (ESI†). A schematic illustration of the TSC structure and the corresponding cross-sectional SEM image are shown in Fig. 5a and b, respectively. Our 2T all-perovskite TSCs have a champion efficiency of 26.68 (26.64)%, with a V_{OC} of 2.115 (2.107) V, a J_{SC} of 15.29 (15.41) mA cm^{-2}, and a FF of 82.5 (82.1)% under reverse (forward) scans. However, the control TSC presents a relatively lower performance of 25.14 (24.98)%, with a V_{OC} of 2.041 (2.039) V, a J_{SC} of 15.13 (15.10) mA cm^{-2}, and a FF of 81.4 (81.1)% under reverse (forward) scans (Fig. 5c).

The EQE-integrated J_{SC}s of the corresponding top and bottom subcells in an optimized TSC are 15.7 mA cm^{-2} and 15.0 mA cm^{-2}, respectively, showing a higher current density than the control one (Fig. 5d). As shown in Fig. 5e, the 2T all-perovskite TSC exhibits a stabilized PCE of 26.6% measured by MPP tracking, which is among the state-of-the-art all-perovskite TSCs.[12,13,51,68] The control one presents an inferior PCE of 25.0%. Moreover, our 2T all-perovskite TSCs are reproducible with an averaged PCE of 25.85 ± 0.84% upon $PbCl_2$ + PMACl treatments, while the control TSCs have an averaged PCE only of 24.13 ± 0.97% (Fig. 5f).

We further tested the operational stability of our 2T TSCs under continuous 1 sun illumination in a glovebox, as shown in Fig. 5g. The unencapsulated $PbCl_2$ + PMACl TSC presents improved stability of retaining 85% of its original PCE after 300 h, while the control one declines to around 72% after 280 h. The improved operational stability of the $PbCl_2$ + PMACl tandem device can be related to the reduced trap density and suppressed phase segregation in the wide-E_g perovskite subcell.

3. Conclusion

We have uncovered the synergistic effects of $PbCl_2$ and PMACl on improving the performance of wide-E_g PSCs as precursor additives. $PbCl_2$ + PMACl facilitates the formation of triple halide compositions and leads to the 2D perovskite phase, thus reducing halide vacancies and suppressing phase segregation, which finally enhances the operational and long-term stability of the corresponding PSCs. 1.73 eV wide-E_g PSCs with a champion V_{OC} of 1.312 V were obtained, presenting a V_{OC}-

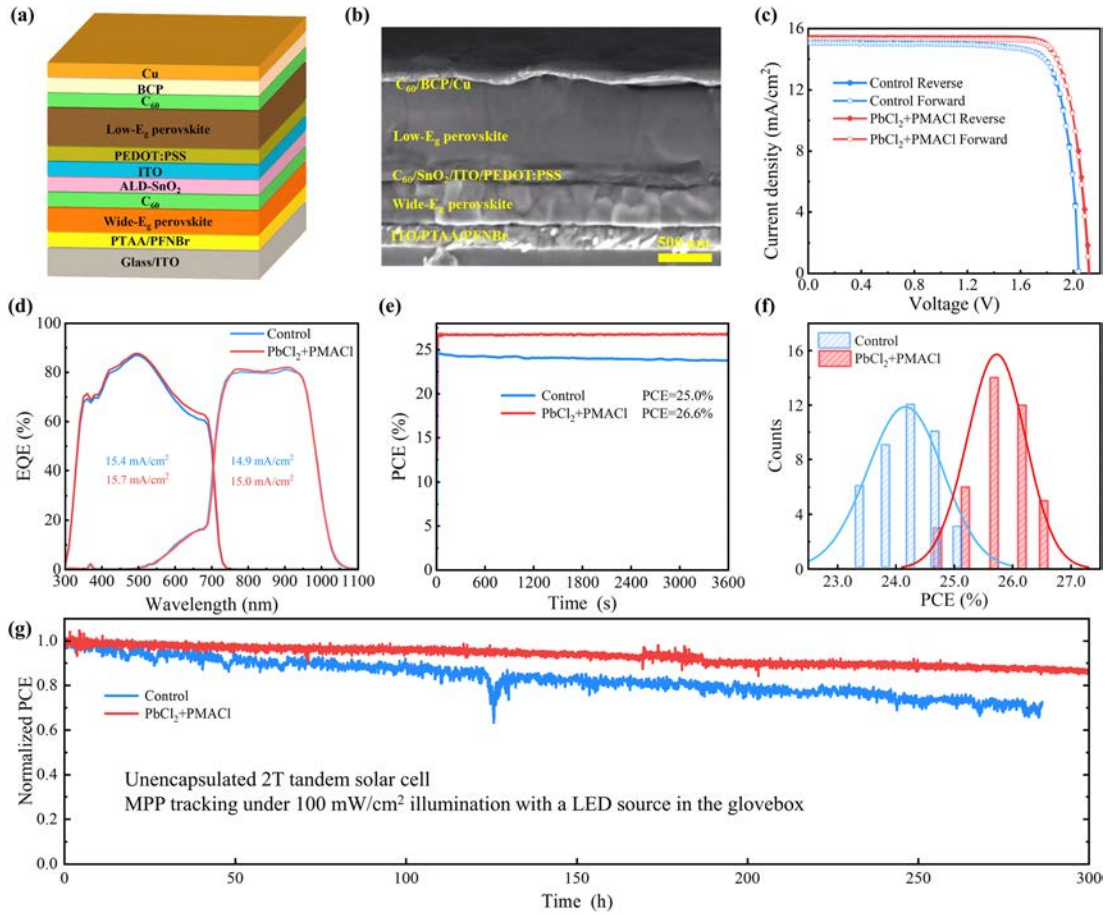

Fig. 5 Photovoltaic performance of 2T all-perovskite TSCs. (a) Schematic structure of a 2T TSC device. (b) Cross-sectional SEM image of one representative 2T TSC. (c) *J*–*V* curves of the control and $PbCl_2$ + PMACl 2T TSCs measured under reverse and forward voltage scans. (d) EQE spectra of the top and bottom subcells in the control and $PbCl_2$ + PMACl 2T TSCs. (e) Power outputs for the control and $PbCl_2$ + PMACl 2T TSCs by MPP tracking. (f) PCE histograms of the control and $PbCl_2$ + PMACl 2T TSCs (40 devices in count). (g) Normalized PCEs under MPP tracking for the control and $PbCl_2$ + PMACl 2T TSCs. The devices without encapsulation were measured under inert conditions and under 100 mW cm^{-2} illumination with a LED light source.

deficit as low as 0.418 V, which is among the lowest values for inverted wide-E_g PSCs reported so far. Moreover, 2T all-perovskite TSCs achieve a champion PCE of 26.68% and an excellent stability of 85% upon MPP tracking for 300 h. Our strategy provides a facile way for fabricating high-performance wide-E_g PSCs and all-perovskite TSCs with reduced defects and suppressed phase segregation.

Conflicts of interest

The authors declare no competing interests.

Acknowledgements

This work was financially supported by the National Key R&D Program of China (No. 2022YFB4200303 and 2022YFB4200900), the National Natural Science Foundation of China (No. 62005188, 62174112, and 62120106001), the Natural Science Foundation of Jiangsu Province (BK20190825), the Natural Science Research Project of Jiangsu Higher Education Institutions (22KJA480003), the Fundamental Research Funds for the Central Universities (No. 2021SCU1205 and YJ201955), the Engineering Featured Team Fund of Sichuan University (2020SCUNG102), and Open Project of Engineering Research Center of Alternative Energy Materials & Devices, Ministry of Education, Sichuan University (AEMD202202).

References

1 J. Peng, D. Walter, Y. Ren, M. Tebyetekerwa, Y. Wu, T. Duong, Q. Lin, J. Li, T. Lu, M. A. Mahmud, O. L. C. Lem, S. Zhao, W. Liu, Y. Liu, H. Shen, L. Li, F. Kremer, H. T. Nguyen, D.-Y. Choi, K. J. Weber, K. R. Catchpole and T. P. White, *Science*, 2021, **371**, 390–395.
2 J. J. Yoo, G. Seo, M. R. Chua, T. G. Park, Y. Lu, F. Rotermund, Y.-K. Kim, C. S. Moon, N. J. Jeon, J.-P. Correa-Baena, V. Bulović, S. S. Shin, M. G. Bawendi and J. Seo, *Nature*, 2021, **590**, 587–593.
3 NREL, Best Research-Cell Efficiencies, 2023, **https://www.nrel.gov/pv/cell-efficiency.html**.
4 W. Shockley and H. J. Queisser, *J. Appl. Phys.*, 1961, **32**, 510–519.
5 Z. Yu, M. Leilaeioun and Z. Holman, *Nat. Energy*, 2016, **1**, 16137.
6 Y. An, T. Ma and X. Li, *Sol. RRL*, 2021, **5**, 2100199.
7 J. Tong, Q. Jiang, F. Zhang, S. B. Kang, D. H. Kim and K. Zhu, *ACS Energy Lett.*, 2020, **6**, 232–248.
8 C. Wang, Z. Song, C. Li, D. Zhao and Y. Yan, *Adv. Funct. Mater.*, 2019, **29**, 1808801.
9 Z. Song, C. Chen, C. Li, R. A. Awni, D. Zhao and Y. Yan, *Semicond. Sci. Technol.*, 2019, **34**, 093001.
10 M. Anaya, G. Lozano, M. E. Calvo and H. Míguez, *Joule*, 2017, **1**, 769–793.
11 S. Gu, R. Lin, Q. Han, Y. Gao, H. Tan and J. Zhu, *Adv. Mater.*, 2020, **32**, 1907392.
12 R. Lin, J. Xu, M. Wei, Y. Wang, Z. Qin, Z. Liu, J. Wu, K. Xiao, B. Chen, S. M. Park, G. Chen, H. R. Atapattu, K. R. Graham, J. Xu, J. Zhu, L. Li, C. Zhang, E. H. Sargent and H. Tan, *Nature*, 2022, **603**, 73–78.
13 K. Xiao, Y.-H. Lin, M. Zhang, R. D. J. Oliver, X. Wang, Z. Liu, X. Luo, J. Li, D. Lai, H. Luo, R. Lin, J. Xu, Y. Hou, H. J. Snaith and H. Tan, *Science*, 2022, **376**, 762–767.
14 W. Chen, Y. Zhu, J. Xiu, G. Chen, H. Liang, S. Liu, H. Xue, E. Birgersson, J. W. Ho, X. Qin, J. Lin, R. Ma, T. Liu, Y. He, A. M.-C. Ng, X. Guo, Z. He, H. Yan, A. B. Djurišić and Y. Hou, *Nat. Energy*, 2022, **7**, 229–237.
15 Z. Guo, A. K. Jena, G. Kim and T. Miyasaka, *Energy Environ. Sci.*, 2022, **15**, 3171–3222.
16 G. Yang, Z. Ni, Z. J. Yu, B. W. Larson, Z. Yu, B. Chen, A. Alasfour, X. Xiao, J. M. Luther, Z. C. Holman and J. Huang, *Nat. Photonics*, 2022, **16**, 588–594.
17 H. Chen, A. Maxwell, C. Li, S. Teale, B. Chen, T. Zhu, E. Ugur, G. Harrison, L. Grater, J. Wang, Z. Wang, L. Zeng, S. M. Park, L. Chen, P. Serles, R. A. Awni, B. Subedi, X. Zheng, C. Xiao, N. J. Podraza, T. Filleter, C. Liu, Y. Yang, J. M. Luther, S. De Wolf, M. G. Kanatzidis, Y. Yan and E. H. Sargent, *Nature*, 2023, **613**, 676–681.
18 J. Xu, C. C. Boyd, Z. J. Yu, A. F. Palmstrom, D. J. Witter, B. W. Larson, R. M. France, J. Werner, S. P. Harvey, E. J. Wolf, W. Weigand, S. Manzoor, M. F. A. M. van Hest, J. J. Berry, J. M. Luther, Z. C. Holman and M. D. McGehee, *Science*, 2020, **367**, 1097–1104.
19 J. Y. Ye, J. Tong, J. Hu, C. Xiao, H. Lu, S. P. Dunfield, D. H. Kim, X. Chen, B. W. Larson, J. Hao, K. Wang, Q. Zhao, Z. Chen, H. Hu, W. You, J. J. Berry, F. Zhang and K. Zhu, *Sol. RRL*, 2020, **4**, 2000082.
20 A. Al-Ashouri, E. Köhnen, B. Li, A. Magomedov, H. Hempel, P. Caprioglio, J. A. Márquez, A. B. Morales Vilches, E. Kasparavicius, J. A. Smith, N. Phung, D. Menzel, M. Grischek, L. Kegelmann, D. Skroblin, C. Gollwitzer, T. Malinauskas, M. Jošt, G. Matič, B. Rech, R. Schlatmann, M. Topič, L. Korte, A. Abate, B. Stannowski, D. Neher, M. Stolterfoht, T. Unold, V. Getautis and S. Albrecht, *Science*, 2020, **370**, 1300–1309.
21 C. Chen, Z. Song, C. Xiao, R. A. Awni, C. Yao, N. Shrestha, C. Li, S. S. Bista, Y. Zhang, L. Chen, R. J. Ellingson, C.-S. Jiang, M. Al-Jassim, G. Fang and Y. Yan, *ACS Energy Lett.*, 2020, **5**, 2560–2568.
22 R. Azmi, E. Ugur, A. Seitkhan, F. Aljamaan, A. S. Subbiah, J. Liu, G. T. Harrison, M. I. Nugraha, M. K. Eswaran, M. Babics, Y. Chen, F. Xu, T. G. Allen, A. U. Rehman, C.-L. Wang, T. D. Anthopoulos, U. Schwingenschlögl, M. D. Bastiani, E. Aydin and S. D. Wolf, *Science*, 2022, **376**, 73–77.
23 D. Luo, W. Yang, Z. Wang, A. Sadhanala, Q. Hu, R. Su, R. Shivanna, G. F. Trindade, J. F. Watts, Z. Xu, T. Liu, K. Chen, F. Ye, P. Wu, L. Zhao, J. Wu, Y. Tu, Y. Zhang, X. Yang, W. Zhang, R. H. Friend, Q. Gong, H. J. Snaith and R. Zhu, *Science*, 2018, **360**, 1442–1446.
24 G. Grancini and M. K. Nazeeruddin, *Nat. Rev. Mater.*, 2019, **4**, 4–22.
25 M. Vasilopoulou, A. Fakharuddin, A. G. Coutsolelos, P. Falaras, P. Argitis, A. R. B. M. Yusoff and M. K. Nazeeruddin, *Chem. Soc. Rev.*, 2020, **49**, 4496–4526.

26 F. Zheng, C. Zuo, M. Niu, C. Zhou, S. J. Bradley, C. R. Hall, W. Xu, X. Wen, X. Hao, M. Gao, T. A. Smith and K. P. Ghiggino, *ACS Energy Lett.*, 2020, **12**, 25980–25990.
27 H. Chen, Y. Xia, B. Wu, F. Liu, T. Niu, L. Chao, G. Xing, T. Sum, Y. Chen and W. Huang, *Nano Energy*, 2019, **56**, 373–381.
28 Z. Wang, J. Jin, Y. Zheng, X. Zhang, Z. Zhu, Y. Zhou, X. Cui, J. Li, M. Shang, X. Zhao, S. Liu and Q. Tai, *Adv. Energy Mater.*, 2021, **11**, 2102169.
29 K. Xiao, R. Lin, Q. Han, Y. Hou, Z. Qin, H. T. Nguyen, J. Wen, M. Wei, V. Yeddu, M. I. Saidaminov, Y. Gao, X. Luo, Y. Wang, H. Gao, C. Zhang, J. Xu, J. Zhu, E. H. Sargent and H. Tan, *Nat. Energy*, 2020, **5**, 870–880.
30 S. Hu, K. Otsuka, R. Murdey, T. Nakamura, M. A. Truong, T. Yamada, T. Handa, K. Matsuda, K. Nakano, A. Sato, K. Marumoto, K. Tajima, Y. Kanemitsu and A. Wakamiya, *Energy Environ. Sci.*, 2022, **15**, 2096–2107.
31 Q. Jiang, J. Tong, Y. Xian, R. A. Kerner, S. P. Dunfield, C. Xiao, R. A. Scheidt, D. Kuciauskas, X. Wang, M. P. Hautzinger, R. Tirawat, M. C. Beard, D. P. Fenning, J. J. Berry, B. W. Larson, Y. Yan and K. Zhu, *Nature*, 2022, **611**, 278–283.
32 R. He, S. Ren, C. Chen, Z. Yi, Y. Luo, H. Lai, W. Wang, G. Zeng, X. Hao, Y. Wang, J. Zhang, C. Wang, L. Wu, F. Fu and D. Zhao, *Energy Environ. Sci.*, 2021, **14**, 5723–5759.
33 M. Hu, C. Bi, Y. Yuan, Y. Bai and J. Huang, *Adv. Sci.*, 2016, **3**, 1500301.
34 Z. Yang, A. Rajagopal, S. B. Jo, C.-C. Chueh, S. Williams, C.-C. Huang, J. K. Katahara, H. W. Hillhouse and A. K. Y. Jen, *Nano Lett.*, 2016, **16**, 7739–7747.
35 Y. Lin, B. Chen, F. Zhao, X. Zheng, Y. Deng, Y. Shao, Y. Fang, Y. Bai, C. Wang and J. Huang, *Adv. Mater.*, 2017, **29**, 1700607.
36 X. Zheng, B. Chen, J. Dai, Y. Fang, Y. Bai, Y. Lin, H. Wei, X. C. Zeng and J. Huang, *Nat. Energy*, 2017, **2**, 17102.
37 R. J. Stoddard, A. Rajagopal, R. L. Palmer, I. L. Braly, A. K. Y. Jen and H. W. Hillhouse, *ACS Energy Lett.*, 2018, **3**, 1261–1268.
38 K. A. Bush, K. Frohna, R. Prasanna, R. E. Beal, T. Leijtens, S. A. Swifter and M. D. McGehee, *ACS Energy Lett.*, 2018, **3**, 428–435.
39 D. B. Khadka, Y. Shirai, M. Yanagida, T. Noda and K. Miyano, *ACS Appl. Mater. Interfaces*, 2018, **10**, 22074–22082.
40 R. Lin, K. Xiao, Z. Qin, Q. Han, C. Zhang, M. Wei, M. I. Saidaminov, Y. Gao, J. Xu, M. Xiao, A. Li, J. Zhu, E. H. Sargent and H. Tan, *Nat. Energy*, 2019, **4**, 864–873.
41 C. Chen, Z. Song, C. Xiao, D. Zhao, N. Shrestha, C. Li, G. Yang, F. Yao, X. Zheng, R. J. Ellingson, C.-S. Jiang, M. Al-Jassim, K. Zhu, G. Fang and Y. Yan, *Nano Energy*, 2019, **61**, 141–147.
42 Y. Chen, W. Tang, Y. Wu, R. Yuan, J. Yang, W. Shan, S. Zhang and W.-H. Zhang, *Sol. RRL*, 2020, **4**, 2000344.
43 Z. Li, J. Zhang, S. Wu, X. Deng, F. Li, D. Liu, C. C. Lee, F. Lin, D. Lei, C.-C. Chueh, Z. Zhu and A. K.-Y. Jen, *Nano Energy*, 2020, **78**, 105377.
44 F. Sadegh, S. Akin, M. Moghadam, R. Keshavarzi, V. Mirkhani, M. A. Ruiz-Preciado, E. Akman, H. Zhang, M. Amini, S. Tangestaninejad, I. Mohammadpoor-Baltork, M. Graetzel, A. Hagfeldt and W. Tress, *Adv. Funct. Mater.*, 2021, **31**, 2102237.
45 C. Chen, J. Liang, J. Zhang, X. Liu, X. Yin, H. Cui, H. Wang, C. Wang, Z. Li, J. Gong, Q. Lin, W. Ke, C. Tao, B. Da, Z. Ding, X. Xiao and G. Fang, *Nano Energy*, 2021, **90**, 106608.
46 L. Li, Y. Wang, X. Wang, R. Lin, X. Luo, Z. Liu, K. Zhou, S. Xiong, Q. Bao, G. Chen, Y. Tian, Y. Deng, K. Xiao, J. Wu, M. I. Saidaminov, H. Lin, C.-Q. Ma, Z. Zhao, Y. Wu, L. Zhang and H. Tan, *Nat. Energy*, 2022, **7**, 708–717.
47 J. Wen, Y. Zhao, Z. Liu, H. Gao, R. Lin, S. Wan, C. Ji, K. Xiao, Y. Gao, Y. Tian, J. Xie, C. J. Brabec and H. Tan, *Adv. Mater.*, 2022, **34**, 2110356.
48 Z. Wang, Q. Wei, X. Liu, L. Liu, X. Tang, J. Guo, S. Ren, G. Xing, D. Zhao and Y. Zheng, *Adv. Funct. Mater.*, 2021, **31**, 2008404.
49 S. Gharibzadeh, P. Fassl, I. M. Hossain, P. Rohrbeck, M. Frericks, M. Schmidt, T. Duong, M. R. Khan, T. Abzieher, B. A. Nejand, F. Schackmar, O. Almora, T. Feeney, R. Singh, D. Fuchs, U. Lemmer, J. P. Hofmann, S. A. L. Weber and U. W. Paetzold, *Energy Environ. Sci.*, 2021, **14**, 5875–5893.
50 Y. Zhang, Z. Zhou, F. Ji, Z. Li, G. Cui, P. Gao, E. Oveisi, M. K. Nazeeruddin and S. Pang, *Adv. Mater.*, 2018, **30**, 1707143.
51 J. Tong, Q. Jiang, A. J. Ferguson, A. F. Palmstrom, X. Wang, J. Hao, S. P. Dunfield, A. E. Louks, S. P. Harvey, C. Li, H. Lu, R. M. France, S. A. Johnson, F. Zhang, M. Yang, J. F. Geisz, M. D. McGehee, M. C. Beard, Y. Yan, D. Kuciauskas, J. J. Berry and K. Zhu, *Nat. Energy*, 2022, **7**, 642–651.
52 J. Han, C. Liu, Y. Zhang, Y. Guan, X. Zhang, W. Yu, Z. Tang, Y. Liang, C. Wu, S. Zheng and L. Xiao, *Adv. Opt. Mater.*, 2022, **10**, 2201431.
53 K. B. Lohmann, S. G. Motti, R. D. J. Oliver, A. J. Ramadan, H. C. Sansom, Q. Yuan, K. A. Elmestekawy, J. B. Patel, J. M. Ball, L. M. Herz, H. J. Snaith and M. B. Johnston, *ACS Energy Lett.*, 2022, **7**, 1903–1911.
54 J. Liang, X. Hu, C. Wang, C. Liang, C. Chen, M. Xiao, J. Li, C. Tao, G. Xing, R. Yu, W. Ke and G. Fang, *Joule*, 2022, **6**, 816–833.
55 J. Wang, W. Li and W.-J. Yin, *Adv. Mater.*, 2020, **32**, 1906115.
56 N. Li, S. Tao, Y. Chen, X. Niu, C. K. Onwudinanti, C. Hu, Z. Qiu, Z. Xu, G. Zheng, L. Wang, Y. Zhang, L. Li, H. Liu, Y. Lun, J. Hong, X. Wang, Y. Liu, H. Xie, Y. Gao, Y. Bai, S. Yang, G. Brocks, Q. Chen and H. Zhou, *Nat. Energy*, 2019, **4**, 408–415.
57 E. T. Hoke, D. J. Slotcavage, E. R. Dohner, A. R. Bowring, H. I. Karunadasa and M. D. McGehee, *Chem. Sci.*, 2015, **6**, 613–617.
58 T. Bu, J. Li, H. Li, C. Tian, J. Su, G. Tong, L. K. Ono, C. Wang, Z. Lin, N. Chai, X.-L. Zhang, J. Chang, J. Lu, J. Zhong, W. Huang, Y. Qi, Y.-B. Cheng and F. Huang, *Science*, 2021, **372**, 1327–1332.
59 C. Li, Z. Song, D. Zhao, C. Xiao, B. Subedi, N. Shrestha, M. M. Junda, C. Wang, C.-S. Jiang, M. Al-Jassim, R. J. Ellingson, N. J. Podraza, K. Zhu and Y. Yan, *Adv. Energy Mater.*, 2018, **9**, 1803135.
60 D. Zhao, C. Chen, C. Wang, M. M. Junda, Z. Song, C. R. Grice, Y. Yu, C. Li, B. Subedi, N. J. Podraza, X. Zhao,

G. Fang, R.-G. Xiong, K. Zhu and Y. Yan, *Nat. Energy*, 2018, **3**, 1093–1100.

61 Y. Bai, Z. Huang, X. Zhang, J. Lu, X. Niu, Z. He, C. Zhu, M. Xiao, Q. Song, X. Wei, C. Wang, Z. Cui, J. Dou, Y. Chen, F. Pei, H. Zai, W. Wang, T. Song, P. An, J. Zhang, J. Dong, Y. Li, J. Shi, H. Jin, P. Chen, Y. Sun, Y. Li, H. Chen, Z. Wei, H. Zhou and Q. Chen, *Science*, 2022, **378**, 747–754.

62 X. Lin, H. Su, S. He, Y. Song, Y. Wang, Z. Qin, Y. Wu, X. Yang, Q. Han, J. Fang, Y. Zhang, H. Segawa, M. Grätzel and L. Han, *Nat. Energy*, 2022, **7**, 520–527.

63 R. A. Awni, Z. Song, C. Chen, C. Li, C. Wang, M. A. Razooqi, L. Chen, X. Wang, R. J. Ellingson, J. V. Li and Y. Yan, *Joule*, 2020, **4**, 644–657.

64 D. Zhao, Y. Yu, C. Wang, W. Liao, N. Shrestha, C. R. Grice, A. J. Cimaroli, L. Guan, R. J. Ellingson, K. Zhu, X. Zhao, R.-G. Xiong and Y. Yan, *Nat. Energy*, 2017, **2**, 17018.

65 C. Wang, D. Zhao, C. R. Grice, W. Liao, Y. Yu, A. Cimaroli, N. Shrestha, P. J. Roland, J. Chen, Z. Yu, P. Liu, N. Cheng, R. J. Ellingson, X. Zhao and Y. Yan, *J. Mater. Chem. A*, 2016, **4**, 12080–12087.

66 S. Sidhik, Y. Wang, M. De Siena, R. Asadpour, A. J. Torma, T. Terlier, K. Ho, W. Li, A. B. Puthirath, X. Shuai, A. Agrawal, B. Traore, M. Jones, R. Giridharagopal, P. M. Ajayan, J. Strzalka, D. S. Ginger, C. Katan, M. A. Alam, J. Even, M. G. Kanatzidis and A. D. Mohite, *Science*, 2022, **377**, 1425–1430.

67 X. Zhao, T. Liu, Q. C. Burlingame, T. Liu, R. Holley, G. Cheng, N. Yao, F. Gao and Y.-L. Loo, *Science*, 2022, **377**, eabn5679.

68 Z. Yu, X. Chen, S. P. Harvey, Z. Ni, B. Chen, S. Chen, C. Yao, X. Xiao, S. Xu, G. Yang, Y. Yan, J. J. Berry, M. C. Beard and J. Huang, *Adv. Mater.*, 2022, **34**, 2110351.